MECHANISM OF ACTION OF NITRIFICATION INHIBITORS BASED ON DIMETHYLPYRAZOLE: A MATTER OF CHELATION

Mario Corrochano-Monsalve*[1], Carmen González-Murua[1], Adrián Bozal-Leorri[1], Luis Lezama[2], Beñat Artetxe[2]

[1]Department of Plant Biology and Ecology, Faculty of Science and Technology, University of the Basque Country (UPV/EHU), Leioa, Spain.

[2]Department of Inorganic Chemistry, Faculty of Science and Technology, University of the Basque Country (UPV/EHU), Leioa, Spain.

*Corresponding author: Department of Plant Biology and Ecology, University of the Basque Country-UPV/EHU, Apdo. 644, E-48080 Bilbao, Spain. E-mail address: mario.corrochano@ehu.eus (M. Corrochano-Monsalve).

*Graphical Abstract

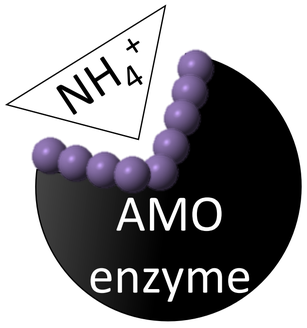

Nitrification

NO_3^- N_2O

Denitrification

N_2O

N_2

X-ray Crystallography

Soil Experiment

NITRIFICATION INHIBITOR

Dimethyl pyrazole (DMP)

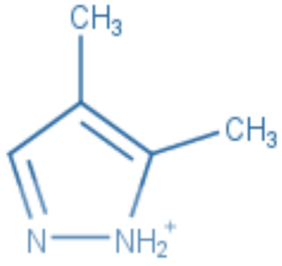

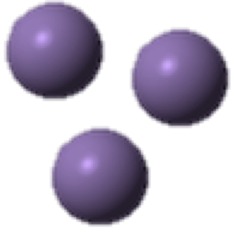

COPPER atoms

Chelation

CuDMP complex

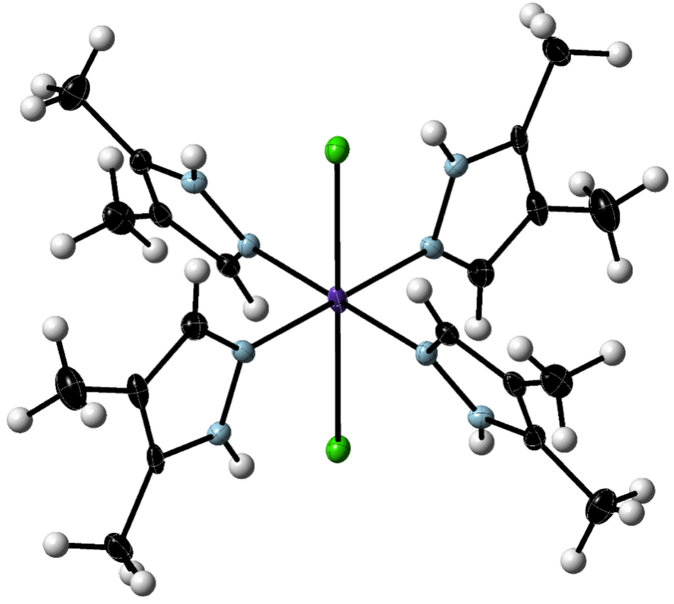

Nitrification Inhibition

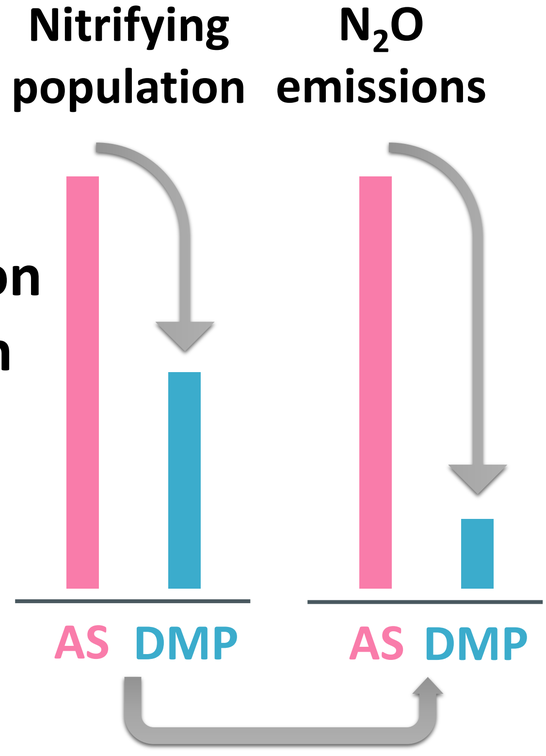

***Highlights (for review : 3 to 5 bullet points (maximum 85 characters including spaces per bullet point)**

- The action of DMPP and DMPSA is tested through chemical and biological studies.
- Nitrification inhibitors (NIs) based on DMP are copper-chelating compounds.
- There is a direct relationship among Zn content, de/nitrification and the use of NIs.
- Both NIs minimize N_2O emissions in soils with different Cu and Zn contents.
- The amount of metals in the soil influence the pathway for the reduction of emissions.

ABSTRACT

In agriculture, the applied nitrogen (N) can be lost in the environment in different forms because of microbial transformations. It is of special concern the nitrate (NO_3^-) leaching and the nitrous oxide (N_2O) emissions, due to their negative environmental impacts. Nitrification inhibitors (NIs) based on dimethylpyrazole (DMP) are applied worldwide in order to reduce N losses. These compounds delay ammonium (NH_4^+) oxidation by inhibiting ammonia-oxidizing bacteria (AOB) growth. However, their mechanism of action has not been demonstrated, which represent an important lack of knowledge to use them correctly. In this work, through chemical and biological analysis, we unveil the mechanism of action of the commonly applied 3,4-dimethyl-1H-pyrazole dihydrogen phosphate (DMPP) and the new DMP-based NI, 2-(3,4-dimethylpyrazole-1-YL)-succinic acid (DMPSA). Our results show that DMP and DMPSA form complexes with copper (Cu^{2+}) cations, an indispensable cofactor in the nitrification pathway. Three coordination compounds namely $[Cu(DMP)_4Cl_2]$ (**CuDMP1**), $[Cu(DMP)_4SO_4]_n$ (**CuDMP2**) and $[Cu(DMPSA)_2]\cdot H_2O$ (**CuDMPSA**) have been synthesized and chemical and structurally characterized. The CuDMPSA complex is more stable than those containing DMP ligands; however, both NIs show the same nitrification inhibition efficiency in soils with different Cu contents, suggesting that the active specie in both cases is DMP. Our soil experiment reveals that the usual application dose is enough to inhibit nitrification within the range of Cu and Zn contents present in agricultural soils, although their effects vary depending on the content of these elements. As a result of AOB inhibition by these NIs, N_2O-reducing bacteria seem to be beneficed in Cu-limited soils due to a reduction in the competence. This opens up the possibility to induce N_2O reduction to N_2 through Cu fertilization. On the other hand, when fertilizing with micronutrients such as Cu and Zn, the use of NIs could be beneficial to counteract the increase of nitrification derived from their application.

1. INTRODUCTION

The third most abundant greenhouse gas (GHG) in the atmosphere, behind carbon dioxide (CO_2) and methane (CH_4), is nitrous oxide (N_2O) (Montzka et al., 2011). The

environmental impact of N_2O emission is drastic due to its global warming potential (GWP), 265 times higher than CO_2 (IPCC, 2014), and its role in stratospheric ozone depletion through nitric oxide (NO) formation (Ravishankara et al., 2009).

Agriculture produces large amounts of nitrate (NO_3^-) leaching and N_2O emissions because of nitrogen fertilization. Ammonium (NH_4^+) based fertilizers applied to soils are biologically transformed through a chain of redox reactions catalyzed by several enzymes (Arp et al., 2003) that contain a variety of transition metals as cofactors or catalytic centers (Glass and Orphan, 2012; Pauleta et al., 2013). The final product of these reactions is molecular nitrogen (N_2), a harmless and inert gas. However, this transformation is not always complete and different intermediate compounds are produced. First, NH_4^+ is oxidized to hydroxylamine (NH_2OH) and to nitrite (NO_2^-) by the action of ammonia-oxidizing archaea (AOA) and ammonia-oxidizing bacteria (AOB) through hydroxylamine oxidoreductase (HAO) and ammonium monooxygenase (AMO) enzymes. AMO contains copper (6 Cu^{2+} and 3 Cu^+ ions), iron (4 Fe^{3+}) and zinc (3 Zn^{2+}) (Gilch et al., 2009a, 2010). The NO_2^- is then oxidized to nitrate (NO_3^-) by nitrite-oxidizing bacteria (NOB). Afterward, nitrogen can be converted into its gaseous forms in the denitrification process. The NO_3^- is sequentially reduced first to NO_2^- by means of nitrate reductase enzyme (NarGH), and then to NO by two different nitrite reductases, NirS (exhibits iron cations) and NirK (displays copper cations). This NO is rapidly transformed into N_2O by means of nitric oxide reductase enzyme (NorBC). Finally, N_2O can be reduced to N_2 by the nitrous oxide reductase (N_2OR), a multi-copper enzyme in which each subunit contains two redox-active copper centers (Pomowski et al., 2011). Along this process, nitrogen can be lost in the form of NO_3^- leaching, due to its lack of adhesion to soil clays, and by N_2O emission coming from nitrifiers denitrification (Wrage et al., 2001; Shaw et al., 2006) and the incomplete reduction of nitrogen-containing gases, because of the absence of N_2OR enzyme in one-third of all denitrifiers (Jones et al., 2008; Philippot et al., 2011). Altogether means that the use of nitrogen in agriculture is not efficient. In fact, it is expected that N_2O emissions from agriculture will account for the 59% of total anthropogenic N_2O emissions in 2030 (Hu et al., 2015). Therefore, it is necessary to develop strategies to improve its sustainability.

Nitrification inhibitors (NIs), such as 3,4-dimethyl-1H-pyrazole dihydrogen phosphate (DMPP) and 2-(3,4-dimethylpyrazole-1-YL)-succinic acid (DMPSA) have been developed to delay NH_4^+ oxidation to NO_3^- by nitrification. This provides plants (crops) with more time to absorb nitrogen, which results in lower NO_3^- leaching and less N_2O emissions without negative effects on crop yield (Di and Cameron, 2012; Guardia et al., 2018a; Huérfano et al., 2018; Recio et al., 2019; Corrochano-Monsalve et al., 2020). Many assumptions have been made with respect to the mechanism of action of DMPP and DMPSA (hereinafter DMPs). Some authors reported that both DMPs act in the same manner, because it is believed that DMPSA molecules need to be decomposed to dimethylpyrazole (DMP) in order to be active as inhibitor (Pacholski et al., 2016). However, the rupture of covalent C–N bonds is unlikely because its bond energy is as high as 305 kJ mol^{-1} (Luo, 2007). In addition, the registration dossier of DMPSA in the European Chemicals Agency (ECHA) reports no biodegradation after 28 days. On the contrary, this same dossier also claims that the degradation of DMPSA into DMP does take place in soils, which may indicate i) the capacity of some microorganisms to carry out this rupture or ii) the strong effect of some other physical parameters such as ultraviolet radiation. Nevertheless, to our knowledge, no studies have been published confirming this issue. In fact, to date, there is no unequivocal evidence for the mode of action of the DMP-based inhibitors. The only reference to this question belongs to a personal communication from Wissemeier included in the review of Ruser and Schulz (2015), in which the ability to chelate Cu^{2+} ions is attributed to DMPP. Furthermore, it has been proposed that this specific copper-chelation capacity of DMP could hinder the activity of AMO by i) coordinating to the enzymatic active site, as it has been reported for some other inhibitors as acetylene and EDTA (Gilch et al., 2009b; 2010), or ii) reducing the bioavailability of copper ions in soils (Duncan et al., 2017). When this question has been addressed in some other publications related to both DMPs, most of them have referred to this unique personal communication (Barrena et al., 2017; Duncan et al., 2017; Torralbo et al., 2017; Beeckman et al., 2018; Guardia et al., 2018b; Montoya et al., 2018; Cassman et al., 2019; Fuertes-Mendizabal et al., 2019; Sheikhi et al., 2020). When it comes to DMPSA, there is no evidence of any kind about its mechanism of action to our knowledge.

In addition, it is not clear why the quantification of genes encoding for some other enzymes that also contain copper, such as NirK and N_2OR, indicate that the application of DMPs does not hinder but even enhances the activity of the organisms carrying these genes. It has been shown that *nosZI* gene (encoding of N_2OR) expression and N_2OR activity are regulated by copper availability (Sullivan et al., 2013; Shen et al., 2020). However, previous studies have reported an induction of *nosZI* after DMPs application (Torralbo et al., 2017; Corrochano-Monsalve et al., 2020). Hence, gaining insights into the mode of action of these NIs is essential to ascertain these questions and for a proper management of its application.

In this work, the mechanisms of action of DMPP and DMPSA were analyzed through two different approaches: 1) we conducted synthetic chemistry experiments in the lab scale and subsequent crystallographic analyses to elucidate the molecular structure of the compounds synthesized. This allowed us to evaluate the chelating capacity of the inhibitors and 2) we determined the relation between the efficiency of DMP-based inhibitors and the content of Cu and Zn in the soil.

2. MATERIALS AND METHODS

2.1 Experiment 1 – Synthesis and structural characterization of metal complexes

All the solvents and reagents were purchased from commercial sources and used without further purification. The 3,4-dimethyl-1H-pyrazole dihydrogen phosphate (DMPP) and the isomeric mixture of 2-(3,4-dimethylpyrazole-1-YL)-succinic acid and 2-(4,5-dimethylpyrazole-1-YL)-succinic acid (DMPSA) were supplied by Eurochem Agro Iberia S. L. and exhibited high purity (> 97%). The infrared spectra (FT-IR) were recorded as KBr pellets on a Shimadzu FTIR−8400S spectrophotometer in the 400−4000 cm^{-1} spectral range. Carbon, hydrogen and nitrogen contents were determined on a Perkin Elmer 2400 CHN analyzer. Thermogravimetric analyses (TGA) were carried out from room temperature to 600 °C at a rate of 5 °C min^{-1} on a Mettler Toledo TGA/SDTA 851^e thermobalance under a 50 cm^3 min^{-1} flow of synthetic air. Powder X-ray diffraction (PXRD) patterns were recorded from 2θ = 5 to 38° (0.038 step size, 30 s per step) using a Philips X'PERT PRO diffractometer operating at 40

kV/40 mA in θ–θ configuration with monochromated CuKα radiation (λ = 1.5418 Å) and a PIXcel detector. X−band EPR measurements were registered on a Bruker ELEXSYS 500 spectrometer equipped with a super-high-Q resonator ER-4123-SHQ and standard Oxford low-temperature devices. For Q-band studies, EPR spectra were recorded on a Bruker EMX system equipped with an ER-510-QT resonator. The magnetic field was calibrated by a NMR probe and the frequency inside the cavity was determined with a Hewlett-Packard 5352B microwave frequency counter. Computer simulation: WINEPR-Simfonia, version 1.5, Bruker Analytische Messtechnik GmbH.

2.1.1 Synthesis of copper(II) complexes with NIs as ligands

$[Cu(DMP)_4Cl_2]$ (CuDMP1). A mixture of $CuCl_2 \cdot 2H_2O$ (17 mg, 0.1 mmol) and 3,4-dimethyl-1H-pyrazole phosphate (38 mg, 0.2 mmol) in water (20 mL) was stirred for 1h at room temperature after adjusting the pH to ca. 5 with aqueous 1M NaOH. Then, the solution was filtered and the blue precipitate formed can be identified as **CuDMP1** on the basis of FTIR spectroscopy. Blue prismatic single-crystals suitable for XRD experiments were only obtained by liquid-liquid diffusion procedure which involves an aqueous solution of $CuCl_2 \cdot 2H_2O$ (pH = 5) and a solution of DMPP in ethanol, using the same amounts of reactants described above. Yield: 18 mg, 70% based on DMPP. Anal. Calcd (Found): C, 46.29 (45.98); H, 6.27 (6.34); N, 21.59 (21.63). IR (cm^{-1}): 1458(s), 1383(m), 1124(s), 1071(s), 998(m), 972(m), 899(w), 875(w), 808(w), 714(w), 634(w), 602(w), 577(w), 546(w).

$[Cu(DMP)_4SO_4]_n$ (CuDMP2). A hot solution of $CuSO_4 \cdot 5H_2O$ (50 mg, 0.2 mmol) and 3,4-dimethyl-1H-pyrazole phosphate (78 mg, 0.4 mmol) in water (20 mL) was stirred for 20 minutes and filtered. The blue precipitate formed can be identified as **CuDMP2** on the basis of FTIR spectroscopy and PXRD. Dark-blue prismatic single-crystals suitable for XRD experiments were only obtained by liquid-liquid diffusion procedure which involves an aqueous solution of $CuSO_4 \cdot 5H_2O$ and a solution of DMPP in ethanol, using the same amounts of reactants described above. Yield: 25 mg, 46% based on DMPP. Anal. Calcd (Found): C, 44.48 (44.92); H, 5.22 (5.10); N, 20.75 (20.69). IR (cm^{-1}): 1593(w), 1528(w), 1448(w), 1389(w),

1350(w), 1317(m), 1126(s), 1061(m), 988(m), 951(w), 883(m), 808(w), 652(w), 633(m), 604(w).

$[Cu(DMPSA)_2]\cdot H_2O$ (CuDMPSA). To 10 mL of an aqueous solution (pH = 5) of $CuSO_4\cdot 5H_2O$ (25 mg, 0.1 mmol), 2-(3,4-dimethyl-1H-pyrazole-1-yl)-succinic acid (42 mg, 0.2 mmol) dissolved in ethanol (10 mL) was added dropwise. This mixture was stirred for 30 min at room temperature, filtered and left to evaporate in an open container at room temperature. Light-blue prismatic crystals suitable for XRD experiments were obtained after two weeks. Yield: 28 mg, 56% based on Cu. Anal. Calcd (Found): C, 42.88 (42.90); H, 4.62 (4.80); N, 11.22 (11.12). IR (cm^{-1}): 2926(s), 1692(s), 1585(s), 1448(w), 1413(m), 1363(w), 1267(w), 1206(m), 921(w), 834(w), 408(w).

2.1.2 X−ray Crystallography

Single−crystal X−ray diffraction data for **CuDMP1**, **CuDMP2**, **CuDMPSA** and **DMPSA** are given in the Supplementary Information (Table S1). Intensity data were collected at 100 K (293 K in the case of **CuDMP2** and **DMPSA**) on an Agilent Technologies Supernova single source diffractometer equipped with MoKα (0.71073 Å) radiation and Eos CCD detector. For **DMPSA** CuKα (1.54184 Å) radiation and Atlas CCD detector were used instead. Data frames were processed (unit cell determination, multi−scan absorption correction, intensity data integration and correction for Lorentz and polarization effects) using the CrysAlis Pro software package (CrysAlis Pro CCD V38.2 and RED; Oxford Diffraction, Ltd.: Oxford, UK, 2009). The structures were solved using OLEX2 (Dolomanov et al., 2009) and refined by full-matrix least-squares based on F^2 with SHELXL–2014/6 (Sheldrick, 2015) as integrated in WinGX (Farrugia, 1999). Thermal vibrations were treated anisotropically for non-H atoms. Hydrogen atoms from the organic ligands were placed in calculated positions and refined using a riding model with standard SHELXL parameters, whereas those belonging to the hydration water molecule in **CuDMPSA** were located in the Fourier map and O–H bond lengths were manually restrained to 0.84(2)Å (DFIX). For **CuDMP2**, sulfur atoms belonging to bridging sulfate groups were disordered over four crystallographic positions with 25% population factors, whereas oxygen

atoms showed 50% occupancy. Organic DMP ligands exhibit statistical N/C disorder (50% occupancy) in 2 and 5 positions of the pyrazole ring. In the case of **CuDMPSA**, two isomers of the DMPSA ligand were found to coexist in the complex: the 2,3-dimethyl (25%) and 3,4-dimethyl (75%) forms as observed from the refinement of the occupancy of the methyl groups without restriction. These populations were fixed in the last refinement cycle.

CCDC1998718 (**CuDMP1**), 1998719 (**CuDMP2**), 1998720 (**CuDMPSA**) and 1998721 (**DMPSA**) contain the supplementary crystallographic data for this paper. These data can be obtained free of charge from The Cambridge Crystallographic Data Centre via www.ccdc.cam.ac.uk/data_request/cif

2.2 Experiment 2 – Pots experiment

2.2.1 Soil sampling and experimental setup

Soil was collected in September 2019, from a 0–30 cm layer of clay loam soil from non-fertilized plots of a rapeseed crop in the Basque Country (Northern Spain), with 43% of sand, 25% of silt and 32% of clay and pH (1:2.5) of 8. The soil was air dried at room temperature. Roots and rocks were removed and the soil was sieved. In order to increase soil's porosity, it was mixed with sand in proportion of 3:1 soil:sand (v:v). After homogenization, it was stored until the start of the experiment. Each pot (21 cm diameter) was filled with a total of 3.5 kg of dry soil. In order to reactivate the soil microorganisms pots were supplied with 500 mg of carbon in the form of glucose and 3 mg of NH_4NO_3 per kg of dry soil (Menéndez et al., 2012; Torralbo et al., 2017), the soil was rehydrated with deionized water and adjusted to a water-filled pore space (WFPS) (Linn and Doran, 1984) of 50% to ensure mixed aerobic and anaerobic conditions. 8 mg Cu kg^{-1} dry soil were applied to Cu-added soils in the form of $CuSO_4$, content that has been already probed as non-toxic for nitrogen-cycle bacteria (He et al., 2018; Shen et al. 2020). In the same manner, 8 mg Zn kg^{-1} dry soil were applied to Zn-added soils in the form of $ZnSO_4$. 15 days after soil activation, deionized water was added to reach 60% WFPS to favor both nitrification and denitrification (Davidson, 1991; Del Prado et al., 2006). Afterward, all pots were fertilized with ammonium sulfate $(NH_4)_2SO_4$ 21% (AS) at a rate

of 63.11 mg N kg^{-1} dry soil (equivalent to 180 kg N ha^{-1}). NIs, 3,4-dimethyl-1H-pyrazole phosphate (DMPP) and 2-(3,4-dimethyl-1H-pyrazole-1-YL)-succinic acid (DMPSA), were applied with the fertilizer as supplied by the manufacturer (granules), Eurochem Agro Iberia S. L (dose of 0.8% of the NH_4^+-N applied with fertilizer) and applied on the surface. Pots were placed in a greenhouse with conditions consisting in 25 ºC and 50% relative humidity (RH) during daytime and 18ºC and 60% RH during nights, with natural environmental light conditions.

2.2.2 N_2O emissions measurements

N_2O soil emissions were measured using the close chamber method (Chadwick et al., 2014). Gas samples were collected along 22 days from fertilization. Sampling frequency was every two days after fertilization (DAF), increasing it to every day between days 5 and 13 for a more precise record of the emission peak. For the collection of the gas, chambers (20 cm diameter) were inserted inside the pot and they were hermetically sealed. Samples were taken just after closing the chamber (t = 0) and after 60 minutes. 20 mL of gas were taken from each chamber and stored at overpressure in pre-evacuated 12 mL glass vials. Then, they were analyzed in a gas chromatograph (GC) (Agilent, 7890A) equipped with an electron capture detector for N_2O analysis. A capillary column (IA KRCIAES 6017:240 °C, 30 m × 320 µm) was used, and samples were injected by means of a headspace auto-sampler (Teledyne Tekmar HT3) connected to the GC. Standards of N_2O were analyzed at the same time. Gas emission rates were calculated taking into account the gas concentration variation from the beginning to the end of the 60 min. Cumulative emissions during the sampling period were estimated using the trapezoidal rule integration (linear interpolation and numerical integration between sampling times) (Levy et al., 2017).

2.2.3 DNA extraction and quantification of nitrifying and denitrifying genes

Soil cores from each treatment were collected at 0–15 cm depth just before fertilizer application and 15 DAF. After homogenization, subsamples were weighted, frozen in liquid

nitrogen and stored at –80 °C until use. DNA was extracted from 0.35 g fresh weight of soil using the PowerSoil DNA Isolation Kit (MO BIO Laboratories, Carlsbad, CA, USA) including some modifications described in Harter et al. (2014). Extracted DNA concentration and quality were determined by spectrophotometry with a NanoDrop® 1000 (Thermo Scientific, Walthman, MA, USA). Quantitative polymerase chain reactions (qPCR) were performed using SYBR® Premix Ex Taq™ II (Takara-Bio Inc.) and gene-specific primers (Supplementary table S2) to amplify and quantify total bacteria abundance (*16S rRNA*), AMO encoding gene (*amoA*) and N_2OR encoding gene (*nosZI*). Each sample was quantified in triplicate using the StepOnePlus™. Real-Time PCR System and data analysis were carried out by StepOnePlus™ Software 2.3 (Thermo Scientific). Standard curves (log gene copies number per reaction volume versus log N) were prepared from serial dilutions of 10^7 to 10^2 gene copies μL^{-1} of linearized plasmids with insertions of the target genes, and the copy number of target genes per gram of dry soil was calculated according to a modified equation detailed by Behrens et al. (2008): [(number of target gene copies per reaction x volume of DNA extracted) / (volume of DNA used per reaction x gram of dry soil extracted)] / DNA concentration.

2.2.4 Statistical analysis

Statistical evaluation of the data was carried out with SPSS (IBM SPSS Statistics for macOS, version 25.0. Armonk, NY: IBM Corp). One-way ANOVA with Duncan's multiple-range test for separation of means ($P < 0.05$) was employed to test the differences in N_2O emissions and genes abundances depending on the variables tested in this work (Soil Cu and Zn contents and nitrification inhibitors application).

3. RESULTS AND DISCUSSION

3.1. Coordinating ability of inhibitors: Synthetic aspects

Focusing on our interest on DMPP and DMPSA inhibitors and their environmental implications, we decided to conduct chemical reactions in the lab-scale to prepare model systems for the activity of these nitrification inhibitors as chelators of metal ions such as Cu^{2+}.

First, we tested the direct reaction between $CuCl_2$ $2H_2O$ and a two-fold excess of DMPP in water at room temperature. From the initial clear solution, the formation of a dark blue precipitate is observed when adjusting the pH to 5 using aqueous 1M NaOH. FT-IR spectroscopy (Supplementary fig. S1A) reveals that this blue precipitate contains DMP molecules in its structure as evidenced by the most intense vibrational bands located at 500-1500 cm^{-1} region that could be ascribed to different stretching and bending modes within the dimethyl imidazole ring (Hasegawa et al., 2000). Coordination of DMP to copper centers can be clearly observed not only in its color, but also when comparing the IR spectrum with that of pure DMPP as observed in related methyl-imidazole systems (Di Santo et al., 2018). To get more insight about this complex, we performed different synthetic modifications for the $CuCl_2$ / DMPP system including i) the screening of the pH of aqueous solutions between 3 and 7; ii) variation of the reaction temperature (room temperature, 50 and 90 ˚C); and iii) the use of ethanol as co-solvent in liquid-liquid diffusion procedures. Fortunately, blue single-crystals (**CuDMP1**) suitable for X-ray diffraction experiments were obtained following the latter approach. In a test tube, a solution of DMPP in ethanol (10 mL) was slowly deposited over an aqueous solution of the Cu^{2+} salt (10 mL), in such a way that two phases are not mixed. Crystals grew in the interphase between both components. As can be observed by FT-IR spectroscopy, the spectrum of **CuDMP1** is virtually identical to that of the powdered sample isolated in the parent reaction. This indicates that DMP easily coordinates to Cu^{2+} in water and suggests that similar processes could be taking place in soils. We tried to confirm if both powder and crystals belong to the same phase but with no success. PXRD experiments carried out for the powdered sample revealed its amorphous nature because no well-defined diffraction maxima can be observed in the XRD pattern.

Analogous experiments to those carried out for the chloride salt were performed for $CuSO_4 \cdot 5H_2O$. The direct reaction between this Cu^{2+} salt and a two-fold excess of DMPP in water afforded a blue precipitate whose FTIR spectrum differs considerably from that of **CuDMP1** (Supplementary fig. S1A). Thus, we tried to get crystals from this reaction by modifying synthetic conditions as described above for the previous system. Similar diffusion

procedures employed for **CuDMP1** yielded crystals of **CuDMP2**, whose FTIR spectrum is virtually identical to that of the powdered, amorphous sample. These observations show that the counterion plays a key role in the formation of different complexes between Cu^{2+} and DMP. Encouraged by all these results, we decided to test whether the coordination of DMP could be observed in other metal ions of interest such as Cu^{+} and Zn^{2+}. A fast oxidation to Cu^{2+} is observed under similar synthetic conditions for the former ion as evidenced by the color change from colorless to blue observed in the aqueous reaction. For Zn^{2+}/DMP system, the IR of the white precipitate formed from the direct aqueous reaction suggests that the inhibitor coordinates to the metal center, because it is virtually identical to that of **CuDMP1**. Unfortunately, no crystal was obtained following similar reaction approaches.

When it comes to the DMPSA inhibitor, its lower solubility in aqueous acidic media (pH = 2 to 5) forced us to select ethanol:water (1:1) mixtures as reaction solvent. The addition of a two-fold excess of DMPSA dissolved in ethanol to an aqueous solution of $CuSO_4 \cdot 5H_2O$ yielded blue light crystals of **CuDMPSA**. The FTIR spectrum of **CuDMPSA** (Supplementary fig. S1B) in comparison to that of pure DMPSA reveals the coordination of DMPSA to copper centers as observed in the blue shift of the most intense vibrational bands located at 1740 and 1648 cm^{-1} that appear at 1692 and 1585 cm^{-1} for **CuDMPSA** and could be ascribed to C-O stretching modes from carboxylate groups. It is worth mentioning that crystals of pure protonated **DMPSA** were isolated when the reaction took place in very acidic medium (pH = 2).

Thermal stability of all the three compounds synthesized was evaluated by TGA/SDTA analyses (Supplementary fig. S2). The endothermic dehydration process for **CuDMPSA** is completed at ~140 °C [calcd (found) for 1 H_2O: 3.48 (3.39)], whereas complexes **CuDMP1** and **CuDMP2** are thermally stable up to ~105 °C and 185 °C respectively. This suggests that the later phases do not exhibit crystallization solvent molecules in their structures. Initial stages are followed by a three-step, highly exothermic ligand combustion, resulting in the final residue above 555 °C, 485 °C and 465 °C for **CuDMP1**, **CuDMP2** and **CuDMPSA**, respectively. The weight percentage of the final residues is in full agreement with the expected value [calcd (found) for CuO: 15.33 (16.11) for **CuDMP1**; 14.73 (16.08) for **CuDMP2**; 15.74 (15.48) for

CuDMPSA]. and the mass loss accounts for at least 4 DMP molecules in the case of **CuDMP1** and **CuDMP2** and 2 DMPSA units per copper center for **CuDMPSA**. This implies that the reaction yield of **CuDMP1** and **CuDMP2** could be considerably improved by adding a larger (four-fold) excess of DMPP instead of the 1:2 Cu^{2+}:DMPP ratio used in this work.

3.2. Crystal structures

Two different compounds were isolated in the reaction between Cu^{2+} salts and the DMPP inhibitor depending on the counterion of the metal source: $CuCl_2$ afforded **CuDMP1**, whereas $CuSO_4$ led to **CuDMP2**. To our knowledge, both represent the first examples in the literature of transition metal complexes containing the DMP ligand. **CuDMP1** (Fig. 1) crystallizes in the triclinic *P*−1 space group and the complex contains one Cu^{2+} cation on an inversion center, exhibiting an axially elongated octahedral coordination geometry. The equatorial plane is formed by four N-donor DMP ligands and the axial positions are occupied by Cl atoms. The crystal packing is formed by monomeric units connected by weak Cl···Cl interactions (3.694(3)Å) that result in one-dimensional arrangements running parallel to the crystallographic *x-axis* (Supplementary fig. S3). **CuDMP2** (Fig. 1) crystallizes in the monoclinic *C*2/*c* space group and it displays Cu^{2+} cations exhibiting axially elongated octahedral coordination geometry. The equatorial plane of each copper center is formed by four N-donor DMP ligands and the axial positions are occupied by O atoms from sulfate groups that act as bridging units between metal centers. These covalent chains run along the crystallographic *y-axis* and their packing strongly resembles that displayed by **CuDMP1** (Supplementary fig. S4).

When it comes to metal complexes containing DMPSA ligands, **CuDMPSA** is completely unprecedented because no examples of such kind of structures can be found in the CSD database. **CuDMPSA** (Fig. 1) crystallizes in the monoclinic $P2_1/c$ space group and the complex contains one Cu^{2+} cation on an inversion center, exhibiting a highly distorted octahedral coordination geometry due to the geometrical restrictions arising from the two deprotonated, tridentate N,O,O'-donor $DMPSA^-$ ligands coordinated to the metal center in *fac*-mode. Equatorial positions are occupied by N atoms from pyrazole rings and O atoms

belonging to the carboxylate groups, whereas axial positions are blocked by O atoms from protonated carboxylic groups. The cell unit also contains one hydration water molecule disordered over two symmetry-related positions showing 50% occupancy. The crystal packing is constituted by supramolecular layers formed by hydrogen bonding parallel to the *yz* plane. Each carboxylic moiety establishes one strong O–H···O interaction (2.54(4)Å) with the analogous group from an adjacent complex, in such a way that each monomer is linked to four neighbors. Two weak C–H···O type contacts between complexes reinforce this arrangement. These layers stack along the crystallographic *x-axis* (Supplementary fig. S5). It is worth mentioning that the DMPSA inhibitor provided by the supplier sources contains two different isomers of the DMPSA ligands: the 2,3-dimethyl and the 3,4-dimethyl forms. The presence of these two isomers can be clearly observed in the structure of **CuDMPSA** which shows 25 % of the former and 75 % of the latter configuration according to XRD data. In the course of the systematic synthetic studies, crystals of pure diprotonated DMPSA (**DMPSA**) were also isolated. The structure of **DMPSA** displays only the 2,3-dimethyl isomer of the inhibitor. These molecules are organized in double chains running along the crystallographic *z-axis*, in which monomers are connected to three neighbors through O–H···O and interaction O–H···N type interactions (2.605(4) and 2.631(%) Å, respectively) established between carboxylic groups and pyrazole rings (Supplementary fig. S6).

3.3. EPR spectroscopy and competitive reactions.

EPR spectroscopy experiments were conducted for all the three compounds synthesized because this sensitive technique could be useful to tentatively identify the formation of these complexes in real samples such as soils. X and Q band EPR measurements for the three complexes were carried out on powdered samples at several temperatures in the range 4–300 K. All the spectra exhibit near axial symmetry for the g tensor in the $\Delta M_s=\pm1$ region, but a slight degree of rhombicity can be deduced from the spectra recorded in Q band (Fig. 2A). The main components of the g tensors were determined by comparison of the experimental spectra with those calculated at a second order of the perturbation theory with a computer simulation

program. Adjusting the observed signals by the trial and error method, the following values were obtained: g_1=2.306, g_2=2.065, g_3=2.061 (g_{II}=2.306, $g_{\perp}$=2.063, <g>=2.144) for compound **CuDMP1**; g_1=2.318, g_2=2.068, g_3=2.060 (g_{II}=2.318, $g_{\perp}$=2.064, <g>=2.149) for compound **CuDMP2**; g_1=2.314, g_2=2.071, g_3=2.065 (g_{II}=2.314, $g_{\perp}$=2.068, <g>=2.150) for compound **CuDMPSA**. These values were used to simulate the powder EPR spectrum in order to produce the dashed line in Fig. 2A. In all cases, the minor g value is higher than 2.04 as expected for mainly $d_x2_{-y}2$ ground states derived from axially elongated octahedral geometries in Cu^{2+} ions (Hathaway and Billing, 1970). The spectrum of **CuDMP2** shows partially resolved hyperfine structure for the nuclear spin of copper (^{65}Cu, ^{63}Cu; I=3/2) on the low field line (A_{II}=181x10^{-4} cm^{-1}), indicating that the intermolecular magnetic exchange pathway is less efficient in this compound in spite of the sulfate bridges. The G parameter as defined by Hathaway has been utilized to confirm the significance of the calculated g values to give any definitive information on the electronic ground state present. For the three complexes the G value lies in the 4.4-5.0 range, therefore the effect of the exchange coupling is negligible and the observed g values are meaningful. Moreover, the spectra remain practically unchanged over the temperature range 4.2-298 K, so the magnetic interactions should be of small magnitude.

Despite the high sensitivity of EPR spectroscopy to detect the presence of paramagnetic ions in different environments, no signal attributable to Cu^{2+} species could be observed in the EPR spectra recorded on *as prepared* soil samples, not even in the presence of DMPP or DMPSA. In order to increase its copper content to analyze the possible formation of chelates with nitrification inhibitors, a weighed amount (500 mg) of dry soil were rehydrated and mixed with different amounts of $CuSO_4$ (0.33, 1, 8 and 32 mg) and the proportional inhibitor amounts. After being stirred, the samples were filtered and dried. Fig. 2B displays the EPR spectra registered with these powders at room temperature. It can be seen that the signal of the **CuDMPSA** chelate can be easily detected for copper contents higher than 12 μmol g^{-1}. Furthermore, it was verified that the signal intensity remained practically constant for more than 72 hours. All in all, taking into account the prepared model systems for the interaction between

Cu^{2+} and NIs and the EPR experiments described above, we have confirmed that i) the DMP formed after the dissociation of DMPP in water and DMPSA can chelate Cu^{2+}ions in soils and ii) DMPSA do not need to decompose to DMP to coordinate to metal centers.

Furthermore, to determine the different kinetics/affinity of both inhibitors towards the formation of copper complexes, we decided to perform additional experiments in which one equivalent of $CuSO_4 \cdot 5H_2O$ (0.1 mmol) and two equivalents (0.2 mmol) of each inhibitor DMPP and DMPSA were mixed in 20 mL of water. The resulting clear solution was left to evaporate at room temperature and a blue powder precipitated out from the mother solution in three days. PXRD analyses of this crystalline powder and its comparison with the simulated patterns from single-crystal X-ray diffraction data for **CuDMP2** and **CuDMPSA** revealed that **CuDMPSA** was exclusively formed because the experimental profile is virtually identical to that of the simulated pattern (Supplementary fig. S7).

Different reasons could be on the origin of this fact: i) Thermodynamics: the complex with the tridentate ligand DMPSA much more stable and hence more difficult to break in comparison to that of the monodentate DMP due to the well-known chelate effect. The chelate effect is the enhanced affinity of polydentate ligands for a metal ion compared to the affinity of a collection of similar non-chelating (monodentate) ligands for the same metal (Martell, 1967). ii) Solubility: we experimentally observed that **CuDMPSA** complex was much more insoluble in water. This could be a major reason for the exclusive isolation of **CuDMPSA** in our experiment and strongly affects the availability of copper ions in soils. iii) Kinetics: although less probable, the formation of **CuDMPSA** complex could be faster than that of **CuDMP**.

3.4 Effects of copper and zinc addition to soil on N_2O emissions

Once it has been demonstrated the ability of both DMPP and DMPSA (hereinafter DMPs) to chelate copper, we decided to conduct a soil experiment to test a possible relationship between the action of these NIs and the soil copper content. Moreover, supported by the different affinity showed through PXRD analysis and the different number of DMP/DMPSA ligands found in the crystalline structures of **CuDMP** complexes and **CuDMPSA**, a differential

420 inhibition efficiency between them was considered as a possibility in soils with high copper
421 content. As our results suggested that DMPs may also be able to coordinate Zn^{2+}, we decided to
422 go deeper into this question testing also the effect of the inhibitors under different zinc contents
423 in soils.

424 Despite being necessary for the enzymatic activity of nitrogen cycle, Cu and Zn are
425 toxic above certain concentrations. Nitrification and denitrification show inhibition with Cu
426 concentrations of about 1000 mg kg^{-1} and 100 mg kg^{-1} respectively (Glass and Orphan, 2012;
427 He et al., 2018). On the other hand, Zn concentrations of about 100 mg kg^{-1} and 230–1000 mg
428 kg^{-1} have been reported as EC50 values (effective concentration to produce a 50% of reduction)
429 for nitrification and denitrification. This tolerance varies with the soil NH_4^+-N content (De
430 Brouwere et al., 2007; Ruyters et al., 2010b; Vasileadis et al., 2012). Thus, Cu and Zn doses
431 supplied in this work have been adjusted to values naturally present in European agricultural
432 soils (Toth et al., 2016; Ballabio et al., 2018) to avoid possible toxicity. Soils were incubated
433 during 15 days after the addition of metal ions and before fertilization in order to allow
434 microbial populations to adapt to the new conditions (He et al., 2018). Based on *16S rRNA* gene
435 abundance in the pre-fertilization period (Fig. 3), we can confirm that neither Cu nor Zn supply
436 affected total bacterial abundance in our experiment.

437 The N_2O emissions of AS treatments showed clear differences when comparing natural
438 and metal-added soils. Daily emissions disclosed that maximum peaks were reached 6 days
439 after fertilization (DAF) in case of "AS" (~37 µg N_2O-N kg^{-1} dry soil day^{-1}) (Fig. 4). However,
440 maximum emission was delayed to 11 DAF in case of "AS+Cu" and "AS+Zn" soils, reaching
441 values of ~89 and 45 µg N_2O-N kg^{-1} dry soil day^{-1} respectively.

442 Copper is one of the cofactors involved in the activity of AMO (Gilch et al., 2009a;
443 Glass and Orphan, 2012) and therefore, there is a direct relationship between Cu availability and
444 nitrification. Previous studies have reported a hormetic effect of Cu addition on nitrification, as
445 Cu contents of ~100 mg kg^{-1} can increase potential nitrification (PNR) (Oorts et al., 2006; Sun
446 et al., 2008; Ruyters et al., 2010a) and AOB abundance (He et al., 2018). This suggests that
447 nitrifying activity may be limited by Cu availability. This seems to be the case in our soil,

448 because the addition of Cu ("AS+Cu") produced a 2.7 fold increase in the total cumulative N_2O
449 emissions with respect to "AS" (Fig. 5). The increase in N_2O emissions should be driven by the
450 growth of AOB populations, as it was accompanied by a 3.6 fold increase in *amoA* gene
451 abundance in "AS+Cu" (Fig. 6A).

452 Some other nitrogen-cycle enzymes also require Cu as cofactor (Glass and Orphan,
453 2012). Therefore, other populations would be expected to be affected as well by Cu addition.
454 Among them, N_2OR has a crucial importance because it is the only enzyme known to date able
455 to reduce N_2O to innocuous N_2. The expression of the encoding gene of N_2OR, *nosZI*, depends
456 on Cu availability (Sullivan et al., 2013) and hence, agricultural soils may present a Cu
457 deficiency to maximize N_2O reduction to N_2 (Richardson et al., 2009; Thomson et al., 2012;
458 Black et al., 2016; Shen et al., 2020). Our findings match with those studies because *nosZI*
459 abundance also increased by 1.4 fold with Cu application (Fig. 6B). The differential increase
460 between *amoA* (3.6 fold) and *nosZI* (1.4 fold) abundances seems to be the reason why emissions
461 have increased in "AS+Cu" with respect to "AS" (2.7 fold), as the enhanced growth of AOB
462 population has not been counteracted with a sufficient increment in populations able to reduce
463 the higher N_2O generation to N_2. We can propose that this smoother response of N_2O-reducers
464 (*nosZI*-holding bacteria) may be explained by the stimulation of AOB population growth, which
465 immobilized an important part of the applied Cu and, therefore, decreased its availability for
466 N_2O-reducers.

467 Although to a lesser extent than Cu, Zn also plays an important role within enzymatic
468 activity of nitrogen cycle. It is believed that Zn may be necessary for nitrifiers denitrification
469 (Glass and Orphan, 2012). Furthermore, it might also be present in AMO, although it is not
470 clear if this presence is just accidental, because this site is occupied by Fe in natural conditions
471 (Gilch et al., 2009a; 2010). Some works have suggested that Cu and Zn may compete by the
472 same binding site in AMO, which undergoes inhibition when Cu is displaced from its active site
473 (Radniecki and Ely, 2008). However, related studies have reported hormetic effects on
474 nitrification due to Zn application at low doses (Radniecki and Ely, 2008; Ruyters et al., 2010a;
475 Chen et al., 2014), suggesting that it does seem to be necessary *per se* for AMO activity. This

476 matches also with the 1.7 fold increase of N_2O emissions observed in "AS+Zn" with respect to
477 "AS" (Fig. 5). The data acquired for the *amoA* gene abundance seem to be enough to link the
478 increase in N_2O emissions with the 4.3 fold increase in "AS+Zn" AOB population with respect
479 to "AS" (Fig. 6A). On the contrary, *nosZI* gene abundance was not statistically affected by Zn
480 application (Fig. 6B). This coincides with previous studies that reported no hormetic effect on
481 denitrification (Ruyters et al., 2010b; Chen et al., 2014) and confirms that Zn does not play any
482 key role in the N_2OR activity.
483
484 *3.5 Relationship between nitrification inhibitors and soil copper and zinc contents*
485 The application of NIs was highly effective, because almost a total elimination of N_2O
486 emissions with respect to AS treatments was observed (Fig. 4 and Fig. 5). Both DMPs showed
487 the same performance. The reduction capacity found in this work is much greater than the
488 values observed for field experiments in the original location of these soils (Corrochano-
489 Monsalve et al., 2020), although it is in line with the values observed in previous experiments
490 carried out in microcosms conditions with soils from the same location (Torralbo et al., 2017).
491 The differences between field and controlled conditions could be attributed to the higher
492 homogeneity of soils in laboratory conditions after all the conditioning processes (rock and root
493 removal, drying, sieving, etc.), which probably facilitates a more homogeneous distribution of
494 fertilizer, NIs and water.
495 Up to date, it has been assumed that DMPs inhibit nitrification through Cu chelation
496 (Barrena et al., 2017; Duncan et al., 2017; Torralbo et al., 2017; Beeckman et al., 2018; Guardia
497 et al., 2018; Montoya et al., 2018; Cassman et al., 2019; Fuertes-Mendizabal et al., 2019;
498 Sheikhi et al., 2020), but this assumption was founded in a personal communication cited in the
499 review of Ruser and Schulz (2015). However, there is no report in the literature that validates
500 this experimentally. To our knowledge, our work is the first demonstration of the capacity of
501 DMPP and DMPSA to chelate Cu (and most likely Zn). With this confirmation, we
502 hypothesized that there could be a relation between the nitrification inhibition efficiency of

503 these compounds and the soil Cu and Zn content, as it has been previously suggested by Duncan
504 et al. (2017).

505 Our results indicate that N_2O emissions from all NIs-treated soils are statistically equal
506 (Fig. 5). In fact, as emissions were higher in "AS+Cu" and "AS+Zn" soils, the percentage of
507 emissions reduction by the NIs was even more drastic in both Cu-added soils (98% DMPP; 97%
508 DMPSA) and Zn-added soils (96% DMPP; 97% DMPSA) in comparison to that observed in
509 natural soils (95% DMPP; 90% DMPSA). This is in concordance with the general trend
510 displayed by NIs which show greater emission reduction as higher is the baseline (Li et al.,
511 2018). Moreover, *amoA* abundance was also statistically equal in all the NIs-treated soils (Fig.
512 6A), in spite of the addition of Cu or Zn addition. Interestingly, the percentage of inhibition of
513 AOB population growth was considerably higher in Cu-added soils (86% DMPP; 85%
514 DMPSA) and Zn-added soils (75% DMPP; 73% DMPSA) than in natural soils (35% DMPP;
515 40% DMPSA). Although the inhibition of N_2O emissions was similar in all the different
516 inhibitor treatments, our results showed that there was a difference in the way it was achieved
517 when comparing natural and metal-added soils. There was a clear increase of *nosZI* gene
518 abundance in natural soils with NIs application (+65% DMPP; +35% DMPSA) with respect to
519 "AS" (Fig. 6B). However, this induction was not replicated in the metal-added soils, but it
520 exhibited an opposite trend because a slight decrease was observed in both Cu (+3% DMPP; –
521 12% DMPSA) and Zn-added soils (–10% DMPP; –27% DMPSA) in comparison to "AS+Cu"
522 and "AS+Zn" respectively. This observation indicates that the total reduction of N_2O emissions
523 in natural soils was attributed to two simultaneous processes: 1) the decline of the size of AOB
524 population, which means a decrease of N_2O generation and, 2) a higher reduction of N_2O to N_2
525 through the increase of the abundance of N_2O-reducers. On the contrary, the reduction of
526 emissions was based only on the decrease of AOB abundance in the case of metal-added soils.

527 Our results seem to support the theory of a chelation-based mechanism for nitrification
528 inhibition. However, in this case, it would be expected that other biological processes with Cu
529 and/or Zn requirements, such as NirK and N_2OR enzymatic activity, would be directly affected
530 as well by DMPs application. In fact, Cu availability can be limiting for NirK activity (Zumft,

1997), although this limitation seems to occur only at very low Cu concentrations (0.9 mg kg^{-1}) (Yang et al., 2015). Previous studies showed that the application of DMPs produces no effects on *nirK* gene abundance (Duan et al., 2017; Torralbo et al., 2017), which could indicate that the remaining available Cu is enough to maintain the activity of NirK. Nevertheless, no convincing reason could be found to explain the observed induction of *nosZ* genes after DMPs application so far (Barrena et al., 2017; Torralbo et al., 2017; Fuertes-Mendizábal et al., 2019; Castellano-Hinojosa et al., 2020; Corrochano-Monsalve et al., 2020), taking into account that the reduction of N_2O to N_2 is not carried out in absence of Cu (Glass and Orphan, 2012; Sullivan et al., 2013). Denitrifiers promote the consumption of NO_3^- rather than N_2O reduction in low Cu environments by shutting down N_2OR activity (Felgate et al., 2012). However, as it was observed for NirK, N_2OR could maintain its function (although slowed down) even at extremely low Cu concentrations, and may also be able to directly use that coordinated to organic ligands (Twining et al., 2007). Previous studies have proposed the addition of Cu with chelating ligands to enhance N_2OR activity when soil Cu content is below 150 mg kg^{-1} (Shen et al., 2020). Altogether, it could mean that Cu content is relatively low in "AS" soils, a great part of it is immobilized by AOB and hence, the N_2OR activity is limited. A similar argumentation has been proposed by Richardson et al. (2009). These observations would be supported by the higher *nosZI* abundance observed in "AS+Cu" in comparison to that of "AS". In the case of "AS+DMPP" and "AS+DMPSA" treatments, Cu is not completely immobilized because the growth of AOB is inhibited. In this manner, Cu remains available for N_2O-reducers, which take advantage of their capacity to use it even when it is bound to the inhibitors. This induction of *nosZI* was not observed in "AS+DMPP+Cu" and "AS+DMPSA+Cu" because the growth of these bacteria was not limited by Cu availability in "AS+Cu".

We propose that the processes that took place in Zn-added soils were different: the application of Zn in "AS+Zn" implied a partial substitution of Cu by Zn in AMO (Radniecki et al., 2008) and as a consequence, more Cu remained available for N_2OR. This seems to be reflected in the slight increase of *nosZI* abundance in "AS+Zn" with respect to "AS". In the case of "AS+DMPP+Zn" and "AS+DMPSA+Zn" treatments, Cu and Zn were chelated by the NIs and

559 thus, they were not available for AOB. As a result, *nosZI* abundance reflected a slight decrease
560 in DMPs+Zn soils with respect to "AS+Zn" due to the negative effects of the higher Zn content
561 in soils on denitrifiers (De Brouwere et al., 2007; Chen et al., 2014).

562 The unique features of N_2OR make this enzyme very attractive from both an ecological
563 and economical point of view. The response of *nosZ* genes to DMPs application may pave the
564 way for the development of inductors of N_2OR activity. Nevertheless, the information that has
565 been obtained at this respect until now is still poor, as it has been focused especially in N_2O.
566 However, there is evidence suggesting that *nos* genes expression is regulated by NO rather than
567 N_2O (Pauleta et al., 2013). Considering that previous studies have shown no effects of DMPs
568 over the abundance of *nirK* and *nirS* (Duan et al., 2017; Torralbo et al., 2017), *norB* should gain
569 interest in future works as responsible for NO transformation to N_2O. In the same way, some
570 other genes that seem to be involved in N_2OR synthesis (i.e. *nosR*, *nosC*, *senC2*, *pcuC*)
571 (Richardson et al., 2009; Sullivan et al., 2013) should be considered to complete the scheme.
572 Most of the studies so far have been developed for pure cultures, and works that analyze the
573 relation between Cu content and N_2O reduction to N_2 in soils are still scarce (Richardson et al.,
574 2009; Shen et al., 2020). Nevertheless, it has been already proposed the application of Cu to
575 soils to favor N_2O reducers (Thomson et al., 2012). Our study confirms that Cu addition
576 increases the abundance of N_2O reducers in soils not receiving NIs. However, Cu application
577 increased even more AOB population, thus resulting in higher N_2O emissions due to enhanced
578 nitrification. In addition, the application of Zn also resulted in higher N_2O emissions, which has
579 been previously reported when applying Zn fertilizers to achieve crop biofortification (Montoya
580 et al., 2018). On the other hand, the application of DMPs can minimize the stimulation of
581 nitrification in Cu/Zn-treated soils while maintaining *nosZI* abundance; thus minimizing N_2O
582 emissions. Therefore, the application of these inhibitors would be especially advisable in soils
583 with high Cu/Zn contents and/or when these metals are added with fertilizers. Nevertheless, it
584 would be necessary to analyze whether the dynamics observed in our work take place in the
585 same way in other soil-moisture conditions

Our work is the first approach to elucidate the mode of action of the NIs based on DMP. Herein, we have demonstrated the Cu^{2+} chelation capacity of DMPP and DMPSA through X-ray crystallography. We can conclude that the effectiveness of DMPs is constant within the thresholds of Cu and Zn contents typically present in agricultural soils (Toth et al., 2016; Ballabio et al., 2018). Therefore, if the mechanism of action is effectively driven by their chelation capacity as it has been suggested, it would be displayed not only on Cu, but also on Zn. Furthermore, our results indicate that the applied concentration of the inhibitors is enough to neutralize a potential extra input of Cu and/or Zn. Besides, DMPs' capacity to counteract the emissions increase derived from Zn application, would support the essentiality of Zn for the activity of AMO.

The inhibitory effect of a Cu chelator on nitrification is related to the stability of the complex formed between the ligands and the Cu (Shi et al., 2015). The tridentate coordination of DMPSA to Cu is more stable than the monodentate bond between DMP and Cu; thus, DMPSA should be more effective. Nevertheless, the inhibitory performance of both DMPP and DMPSA in soils has shown no differences between them, suggesting that, i) DMPSA is really acting as DMP, which would imply that despite the high energy of the covalent C–N bonds, DMPSA is somehow rapidly degraded to DMP in the soil (which would match with the half-life of 1.5–3.3 days registered in ECHA) and/or ii) DMPSA maintains its integrity and thus, its dose could be reduced in comparison to that of DMPP, as its chelation efficiency is higher according to the number of ligands per Cu^{2+} cation observed in XRD structures (Fig. 2).

4. CONCLUSIONS

This is the first demonstration of the capacity of DMPP and DMPSA to form complexes with Cu^{2+} cations. Although DMPSA is able to directly bond with Cu^{2+}, our results suggest that it might be degraded to DMP in soils. In any case, the nitrification inhibition displayed by these compounds seems to be driven by the interaction between them and Cu^{2+}, which is an essential cofactor for the activity of AMO. Moreover, there is evidence to suggest a relationship between DMP and Zn^{2+}, and also an essentiality of this element for AMO activity. Our results also

indicate that N_2O-reducing bacteria growth seems to be limited by Cu availability. These bacteria are benefited by DMPs application, which might be due to a reduction in the competence when AOB growth is inhibited. In this manner, the reduction of N_2O to N_2 is promoted. Moreover, the addition of Cu and/or Zn to soils stimulates AOB growth, leading to an increase in N_2O emissions than can be counteracted by DMPs application. Therefore, further studies should be carried out in field conditions to consider the application of NIs when fertilizing with these micronutrients.

ACKNOWLEDGMENTS

This project was funded by de Spanish Government (RTI2018-094623-B-C21 MCIU/AEI/FEDER, UE), the Basque Government (EJ/GV, IT-932-16) and by EuroChem Agro Iberia S.L.-UPV/EHU 2018.0612. Mario Corrochano-Monsalve holds a grant from the Ministry of Economy and Business of the Spanish Government. Beñat Artetxe thanks EJ/GV (grant IT1291-19). Technical and human support provided by SGIker (UPV/EHU, MICINN, EJ/GV, ERDF and ESF) is gratefully acknowledged.

REFERENCES

Arp, D. J., & Stein, L. Y. (2003). Metabolism of inorganic N compounds by ammonia-oxidizing bacteria. Critical Reviews in Biochemistry and Molecular Biology, 38(6), 471–495. https://doi.org/10.1080/10409230390267446

Ballabio, C., Panagos, P., Lugato, E., et al. (2018). Copper distribution in European topsoils: An assessment based on LUCAS soil survey. Science of the Total Environment, 636, 282–298. https://doi.org/10.1016/j.scitotenv.2018.04.268

Barrena, I., Menéndez, S., Correa-galeote, D., Vega-mas, I., Bedmar, E. J., González-murua, C., & Estavillo, J. M. (2017). Soil water content modulates the effect of the nitrification

639 inhibitor 3,4-dimethylpyrazole phosphate (DMPP) on nitrifying and denitrifying bacteria.
640 Geoderma, 303(April), 1–8. https://doi.org/10.1016/j.geoderma.2017.04.022

641 Beeckman, F., Motte, H., & Beeckman, T. (2018). Nitrification in agricultural soils: impact,
642 actors and mitigation. Current Opinion in Biotechnology, 50, 166–173.
643 https://doi.org/10.1016/j.copbio.2018.01.014

644 Behrens, S., Azizian, M. F., McMurdie, P. J., Sabalowsky, A., Dolan, M. E., Semprini, L., &
645 Spormann, A. M. (2008). Monitoring abundance and expression of "Dehalococcoides"
646 species chloroethene-reductive dehalogenases in a tetrachloroethene-dechlorinating flow
647 column. Applied and Environmental Microbiology, 74(18), 5695–5703.
648 https://doi.org/10.1128/AEM.00926-08

649 Black, A., Hsu, P. C. L., Hamonts, K. E., Clough, T. J., & Condron, L. M. (2016). Influence of
650 copper on expression of nirS, norB and nosZ and the transcription and activity of NIR,
651 NOR and N_2OR in the denitrifying soil bacteria Pseudomonas stutzeri. Microbial
652 Biotechnology, 9(3), 381–388. https://doi.org/10.1111/1751-7915.12352

653 Cassman, N. A., Soares, J. R., Pijl, A., Lourenço, K. S., van Veen, J. A., Cantarella, H., &
654 Kuramae, E. E. (2019). Nitrification inhibitors effectively target N_2O-producing
655 Nitrosospira spp. in tropical soil. Environmental Microbiology, 21(4), 1241–1254.
656 https://doi.org/10.1111/1462-2920.14557

657 Castellano-Hinojosa, A., González-López, J., Vallejo, A. & Bedmar, E.J. (2020). Effect of
658 urease and nitrification inhibitors on ammonia volatilization and abundance of N-cycling
659 genes in an agricultural soil. J. Plant Nutr. Soil Sci., 183: 99-109.
660 doi:10.1002/jpln.201900038

661 Chadwick, D.R., Cardenas, L., Misselbrook, et al. (2014). Optimizing chamber methods for
662 measuring nitrous oxide emissions from plot- based agricultural experiments. Eur. J. Soil

Sci. 65, 295–307. https://doi.org/ 10.1111/ejss.12117

Chen, G. C., Tam, N. F. Y., & Ye, Y. (2014). Does zinc in livestock wastewater reduce nitrous oxide (N_2O) emissions from mangrove soils? Water Research, 65, 402–413. https://doi.org/10.1016/j.watres.2014.08.003

Corrochano-Monsalve, M., Huérfano, X., Menéndez, S., Torralbo, F., Fuertes-Mendizábal, T., Estavillo, J.-M., & González-Murua, C. (2020). Relationship between tillage management and DMPSA nitrification inhibitor efficiency. Science of The Total Environment 718C, 134748. https://doi.org/10.1016/j.scitotenv.2019.134748

Davidson, E.A. (1991). Fluxes of nitrous oxide and nitric oxide from terrestrial ecosystems. In: Rogers, J.E. (Ed.). Microbial production and consumption of greenhouse gases: methane, nitrogen oxides, and halomethanes. American Society of Microbiology, Washington, DC, pp. 219–235.

Del Prado, A., Merino, P., Estavillo, J.M., Pinto, M. & González-Murua, C. (2006). N_2O and NO emissions from different n sources and under a range of soil water contents. Nutr. Cycl. Agroecosyst. 74 (3), 229–243. https://doi.org/10.1007/ s10705-006-9001-6

De Brouwere, K., Hertigers, S., & Smolders, E. (2007). Zinc toxicity on N2O reduction declines with time in laboratory spiked soils and is undetectable in field contaminated soils. Soil Biology and Biochemistry, 39(12), 3167–3176. https://doi.org/10.1016/j.soilbio.2007.07.012

Di, H.J. & Cameron, K.C. (2012). How does the application of different nitrification inhibitors affect nitrous oxide emissions and nitrate leaching from cow urine in grazed pastures?. Soil Use and Management, 28: 54-61. doi:10.1111/j.1475-2743.2011.00373.x

Di Santo, A. Pérez, H., Echeverría, G. A. et al. (2018). Exploring weak intermolecular interactions in thiocyanate-bonded Zn(II) and Cd(II) complexes with methylimidazole:

687 crystal structures, Hirshfeld surface analysis and luminescence properties. RSC Adv.,
688 2018,8, 23891–23902. https://doi.org/10.1039/C8RA04452J

689 Dolomanov, O. V., Bourhis, L. J., Gildea, R. J., Howard, J. A. K., & Puschmann, H. (2009).
690 OLEX2: A complete structure solution, refinement and analysis program. Journal of
691 Applied Crystallography, 42(2), 339–341. https://doi.org/10.1107/S0021889808042726

692 Duan, Y. F., Kong, X. W., Schramm, A., Labouriau, R., Eriksen, J., & Petersen, S. O. (2016).
693 Microbial N transformations and N_2O emission after simulated grassland cultivation:
694 effects of the nitrification inhibitor 3,4-dimethylpyrazole phosphate (DMPP). Applied and
695 environmental microbiology, 83(1), e02019-16. https://doi.org/10.1128/AEM.02019-16

696 Duncan, E. G., O'Sullivan, C. A., Simonsen, A. K., Roper, M. M., Peoples, M. B., Treble, K., &
697 Whisson, K. (2017). The nitrification inhibitor 3,4,-dimethylpyrazole phosphate strongly
698 inhibits nitrification in coarse-grained soils containing a low abundance of nitrifying
699 microbiota. Soil Research, 55(1), 28–37. https://doi.org/10.1071/SR15359

700 European Chemicals Agency (ECHA). EC number: 940-877-5
701 https://echa.europa.eu/da/registration-dossier/-/registered-dossier/11890/1. Visited on
702 02/04/2020.

703 Farrugia., L. J. (1999). WinGX suite for small- molecule single-crystal crystallography
704 DISCUS, a program for diffuse scattering and defect structure simulations ± update
705 PowderX : Windows-95-based program for powder X-ray diffraction data processing. J.
706 Appl. Cryst., 32, 837–838. https://doi.org/10.1107/S0021889899006020

707 Felgate, H., Giannopoulos, G., Sullivan, M. J., et al. (2012). The impact of copper, nitrate and
708 carbon status on the emission of nitrous oxide by two species of bacteria with
709 biochemically distinct denitrification pathways. Environmental Microbiology, 14(7),
710 1788–1800. https://doi.org/10.1111/j.1462-2920.2012.02789.x

711 Fuertes-Mendizábal, T., Huérfano, X., Vega-Mas, I., et al. (2019). Biochar reduces the
712 efficiency of nitrification inhibitor 3,4-dimethylpyrazole phosphate (DMPP) mitigating
713 N_2O emissions. Scientific Reports, 9(1), 2346. https://doi.org/10.1038/s41598-019-38697-
714 2

715 Gilch, S., Meyer, O., & Schmidt, I. (2009a). A soluble form of ammonia monooxygenase in
716 Nitrosomonas europaea. Biological Chemistry, 390(9), 863–873.
717 https://doi.org/10.1515/BC.2009.085

718 Gilch, S., Vogel, M., Lorenz, M. W., Meyer, O., & Schmidt, I. (2009b). Interaction of the
719 mechanism-based inactivator acetylene with ammonia monooxygenase of Nitrosomonas
720 europaea. Microbiology, 155(1), 279–284. https://doi.org/10.1099/mic.0.023721-0

721 Gilch, S., Meyer, O., & Schmidt, I. (2010). Electron paramagnetic studies of the copper and iron
722 containing soluble ammonia monooxygenase from Nitrosomonas europaea. BioMetals,
723 23(4), 613–622. https://doi.org/10.1007/s10534-010-9308-2

724 Glass, J. B., & Orphan, V. J. (2012). Trace metal requirements for microbial enzymes involved
725 in the production and consumption of methane and nitrous oxide. Frontiers in
726 microbiology, 3, 61. https://doi.org/10.3389/fmicb.2012.00061

727 Guardia, G., Sanz-Cobena, A., Sanchez-Martín, L., et al. (2018a). Urea-based fertilization
728 strategies to reduce yield-scaled N oxides and enhance bread-making quality in a rainfed
729 Mediterranean wheat crop. Agriculture, Ecosystems and Environment, 265(May), 421–
730 431. https://doi.org/10.1016/j.agee.2018.06.033

731 Guardia, G., Marsden, K. A., Vallejo, A., Jones, D. L., & Chadwick, D. R. (2018b).
732 Determining the influence of environmental and edaphic factors on the fate of the
733 nitrification inhibitors DCD and DMPP in soil. Science of the Total Environment, 624,
734 1202–1212. https://doi.org/10.1016/j.scitotenv.2017.12.250

735 Hasegawa, K., Ono, T., & Noguchi, T. (2000). Vibrational spectra and ab initio DFT
736 calculations of 4-Methylimidazole and its different protonation forms: infrared and raman
737 markers of the protonation state of a histidine side chain. The Journal of Physical
738 Chemistry B 2000 104 (17), 4253-4265. https://doi.org/10.1021/jp000157d

739 Hathaway, B. J. & Billing, D. E. (1970). The electronic properties and stereochemistry of
740 mono-nuclear complexes of the copper(II) ion. *Coordination Chemistry Reviews*, 5(2),
741 143-207. https://doi.org/10.1016/S0010-8545(00)80135-6

742 Harter, J., Krause, H. M., Schuettler, S., et al. (2014). Linking N_2O emissions from biochar-
743 amended soil to the structure and function of the N-cycling microbial community. ISME
744 Journal, 8(3), 660–674. https://doi.org/10.1038/ismej.2013.160

745 He, H., Liu, H., Shen, T., Wei, S., Dai, J., & Wang, R. (2018). Influence of Cu application on
746 ammonia oxidizers in fluvo-aquic soil. Geoderma, 321(January), 141–150.
747 https://doi.org/10.1016/j.geoderma.2018.01.037

748 Hu, H. W., Chen, D., & He, J. Z. (2015). Microbial regulation of terrestrial nitrous oxide
749 formation: Understanding the biological pathways for prediction of emission rates. FEMS
750 Microbiology Reviews, 39(5), 729–749. https://doi.org/10.1093/femsre/fuv021

751 Huérfano, X., Fuertes-Mendizábal, T., Duñabeitia, M. K., González-Murua, C., Estavillo, J. M.,
752 & Menéndez, S. (2015). Splitting the application of 3,4-dimethylpyrazole phosphate
753 (DMPP): Influence on greenhouse gases emissions and wheat yield and quality under
754 humid Mediterranean conditions. European Journal of Agronomy, 64, 47–57.
755 https://doi.org/10.1016/j.eja.2014.11.008

756 Huérfano, X., Fuertes-Mendizábal, T., Fernández-Diez, K., Estavillo, J. M., González-Murua,
757 C., & Menéndez, S. (2016). The new nitrification inhibitor 3,4-dimethylpyrazole succinic
758 (DMPSA) as an alternative to DMPP for reducing N_2O emissions from wheat crops under

759 humid Mediterranean conditions. European Journal of Agronomy, 80, 78–87.
760 https://doi.org/10.1016/j.eja.2016.07.001

761 Huérfano, X., Estavillo, J. M., Fuertes-Mendizábal, T., Torralbo, F., González-Murua, C., &
762 Menéndez, S. (2018). DMPSA and DMPP equally reduce N_2O emissions from a maize-
763 ryegrass forage rotation under Atlantic climate conditions. Atmospheric Environment,
764 187(June), 255–265. https://doi.org/10.1016/j.atmosenv.2018.05.065

765 IPCC-International Panel on Climate Change (2014). In: Pachauri, R.K., Meyer, L.A. (Eds.),
766 Climate Change 2014: Synthesis Report. Contribution of Working Groups I, II and III to
767 the Fifth Assessment Report of the Intergovernmental Panel on Climate Change [Core
768 Writing Team. IPCC, Geneva, Switzerland, pp. 151.

769 Jones, C. M., Stres, B., Rosenquist, M., & Hallin, S. (2008). Phylogenetic analysis of nitrite,
770 nitric oxide, and nitrous oxide respiratory enzymes reveal a complex evolutionary history
771 for denitrification. Molecular Biology and Evolution, 25(9), 1955–1966.
772 https://doi.org/10.1093/molbev/msn146

773 Levy, P.E., Cowan, N., Van Oijen, M., Famulari, D., Drewer, J. & Skiba, U. (2017). Estimation
774 of cumulative fluxes of nitrous oxide: uncertainty in temporal upscaling and emission
775 factors. Eur. J. Soil Sci. 68 (4), 400–411. https://doi.org/ 10.1111/ejss.12432

776 Li, T, Zhang, W, Yin, J, et al. (2018). Enhanced-efficiency fertilizers are not a panacea for
777 resolving the nitrogen problem. Glob Change Biol. 2018; 24: e511– e521.
778 https://doi.org/10.1111/gcb.13918

779 Linn, D.M., Doran, J.W., 1984. Effect of water-filled pore space on carbon dioxide and nitrous
780 oxide production in tilled and nontilled soils. Soil Sci. Soc. Am. J. 48, 1267–1272.

781 Luo, Y. R., Comprehensive Handbook of Chemical Bond Energies, CRC Press, Boca Raton,
782 FL, 2007.

783 Martell, A.E. The chelate effect. Werner Centennial. January 1, 1967, 272–294.
784 http://doi.org/10.1021/ba-1967-0062.ch019

785 Menéndez, S., Barrena, I., Setien, I., González-Murua, C., Estavillo, J.M., 2012. Efficiency of
786 nitrification inhibitor DMPP to reduce nitrous oxide emissions under different temperature
787 and moisture conditions. Soil Biol. Biochem. 53, 82–89.
788 https://doi.org/10.1016/j.soilbio.2012.04.026.

789 Montoya, M., Castellano-Hinojosa, A., Vallejo, A., Álvarez, J. M., Bedmar, E. J., Recio, J., &
790 Guardia, G. (2018). Zinc fertilizers influence greenhouse gas emissions and nitrifying and
791 denitrifying communities in a non-irrigated arable cropland. Geoderma, 325(January),
792 208–217. https://doi.org/10.1016/j.geoderma.2018.03.035

793 Montzka, S., Dlugokencky, E. & Butler, J. (2011). Non-CO_2 greenhouse gases and climate
794 change. Nature 476, 43–50 (2011). https://doi.org/10.1038/nature10322

795 Oorts, K., Ghesquiere, U., Swinnen, K., & Smolders, E. (2006). Soil properties affecting the
796 toxicity of $CuCl_2$ and $NiCl_2$ for soil microbial processes in freshly spiked soils.
797 Environmental Toxicology and Chemistry, 25(3), 836–844. https://doi.org/10.1897/04-
798 672R.1

799 Pacholski, A., Berger, N., Bustamante, I., Ruser, R., Guardia, G. & Mannheim, T., (2016).
800 Effects of the novel nitrification inhibitor DMPSA on yield, mineral N dynamics and N_2O
801 emissions. In: Proceedings of the 2016 International Nitrogen Initiative Conference,
802 ‘‘Solutions to improve nitrogen use efficiency for the world”, 4–8 December 2016,
803 Melbourne, Australia. http://www.ini2016.com/

804 Pauleta, S. R., Dell’Acqua, S., & Moura, I. (2013). Nitrous oxide reductase. Coordination
805 Chemistry Reviews, 257(2), 332–349. https://doi.org/10.1016/j.ccr.2012.05.026

806 Philippot, L., Andert, J., Jones, C. M., Bru, D., & Hallin, S. (2011). Importance of denitrifiers

807 lacking the genes encoding the nitrous oxide reductase for N_2O emissions from soil.
808 Global Change Biology, 17(3), 1497–1504. https://doi.org/10.1111/j.1365-
809 2486.2010.02334.x

810 Pomowski, A., Zumft, W. G., Kroneck, P. M. H., & Einsle, O. (2011). N_2O binding at a
811 [4Cu:2S] copper–sulphur cluster in nitrous oxide reductase. Nature, 477(7363), 234–237.
812 https://doi.org/10.1038/nature10332

813 Radniecki, T. S., & Ely, R. L. (2008). Zinc chloride inhibition of Nitrosococcus mobilis.
814 Biotechnology and Bioengineering, 99(5), 1085–1095. https://doi.org/10.1002/bit.21672

815 Ravishankara, A. R., Daniel, J. S., & Portmann, R. W. (2009). Nitrous Oxide (N_2O): The
816 dominant ozone-depleting substance emitted in the 21st century. Science, 326(5949), 123
817 LP – 125. https://doi.org/10.1126/science.1176985

818 Recio, J., Alvarez, J.M., Rodriguez-Quijano, M., Vallejo, A., 2019. Nitrification inhibitor
819 DMPSA mitigated N_2O emission and promoted NO sink in rainfed wheat. Environmental
820 Pollution, 245(3), 199–207. https://doi.org/10.1016/j.envpol.2018.10.135

821 Richardson, D., Felgate, H., Watmough, N., Thomson, A., & Baggs, E. (2009). Mitigating
822 release of the potent greenhouse gas N_2O from the nitrogen cycle - could enzymic
823 regulation hold the key? Trends in Biotechnology, 27(7), 388–397.
824 https://doi.org/10.1016/j.tibtech.2009.03.009

825 Ruser, R., & Schulz, R. (2015). The effect of nitrification inhibitors on the nitrous oxide (N_2O)
826 release from agricultural soils-a review. Journal of Plant Nutrition and Soil Science, Vol.
827 178, pp. 171–188. https://doi.org/10.1002/jpln.201400251

828 Ruyters, S., Mertens, J., Springael, D., & Smolders, E. (2010a). Stimulated activity of the soil
829 nitrifying community accelerates community adaptation to Zn stress. Soil Biology and
830 Biochemistry, 42(5), 766–772. https://doi.org/10.1016/j.soilbio.2010.01.012

Ruyters, S., Mertens, J., T'Seyen, I., Springael, D., & Smolders, E. (2010b). Dynamics of the nitrous oxide reducing community during adaptation to Zn stress in soil. Soil Biology and Biochemistry, 42(9), 1581–1587. https://doi.org/10.1016/j.soilbio.2010.05.036

Shaw, L.J., Nicol, G.W., Smith, Z., Fear, J., Prosser, J.I. & Baggs, E.M. (2006), Nitrosospira spp. can produce nitrous oxide via a nitrifier denitrification pathway. Environmental Microbiology, 8: 214-222. doi:10.1111/j.1462-2920.2005.00882.x

Sheikhi, J., Mirsyed Hosseini, H., Etesami, H., & Majidi, A. (2020). Biochar counteracts nitrification inhibitor DMPP–mediated negative effect on spinach (Spinacia oleracea L.) growth. Ecotoxicology and Environmental Safety, 191, 110243. https://doi.org/10.1016/J.ECOENV.2020.110243

Sheldrick, G. M. (2015). SHELXT - Integrated space-group and crystal-structure determination. Acta Crystallographica Section A: Foundations of Crystallography, 71(1), 3–8. https://doi.org/10.1107/S2053273314026370

Shen, W., Xue, H., Gao, N., et al. (2020). Effects of copper on nitrous oxide (N_2O) reduction in denitrifiers and N_2O emissions from agricultural soils. Biology and Fertility of Soils, 56(1), 39–51. https://doi.org/10.1007/s00374-019-01399-y

Shi, Y., Zhang, L., Zhao, M., Xu, X., & Wang, G. (2015). Relationships between stability of Cu complexes and nitrification inhibition effects of corresponding ligands in soils. Acta Agriculturae Scandinavica Section B: Soil and Plant Science, 65(3), 271–278. https://doi.org/10.1080/09064710.2015.1004357

Sullivan, M. J., Gates, A. J., Appia-Ayme, C., Rowley, G., & Richardson, D. J. (2013). Copper control of bacterial nitrous oxide emission and its impact on vitamin B12-Dependent metabolism. Proceedings of the National Academy of Sciences of the United States of America, 110(49), 19926–19931. https://doi.org/10.1073/pnas.1314529110

855 Sun, J.W., Huang, Y.Z., Zhao, L.J., Li, X.F., Gao, W.G. (2008). Effects of copper on
856 nitrification rates in 17 kinds of typical soils in China. Asian J. Ecotoxicol. 3, 513–520 (in
857 Chinese).

858 Thomson, A.J., Giannopoulos, G., Pretty, J., Baggs, E.M., & Richardson, D.J., 2012. Biological
859 sources and sinks of nitrous oxide and strategies to mitigate emissions. Philosophical
860 transactions of the Royal Society of London. Series B, Biological sciences, 367(1593),
861 1157–1168. https://doi.org/10.1098/rstb.2011.0415

862 Tóth, G., Hermann, T., Da Silva, M. R., & Montanarella, L. (2016). Heavy metals in
863 agricultural soils of the European Union with implications for food safety. Environment
864 International, 88, 299–309. https://doi.org/10.1016/j.envint.2015.12.017

865 Torralbo, F., Menéndez, S., Barrena, I., Estavillo, J. M., Marino, D., & González-Murua, C.
866 (2017). Dimethyl pyrazol-based nitrification inhibitors effect on nitrifying and denitrifying
867 bacteria to mitigate N_2O emission. Scientific Reports, 7(1), 1–11.
868 https://doi.org/10.1038/s41598-017-14225-y

869 Twining, B. S., Mylon, S. E., & Benoit, G. (2007). Potential role of copper availability in
870 nitrous oxide accumulation in a temperate lake. Limnology and Oceanography, 52(4),
871 1354–1366. https://doi.org/10.4319/lo.2007.52.4.1354

872 Vasileiadis, S., Coppolecchia, D., Puglisi, E., et al. (2012). Response of Ammonia Oxidizing
873 Bacteria and Archaea to Acute Zinc Stress and Different Moisture Regimes in Soil.
874 Microbial Ecology, 64(4), 1028–1037. https://doi.org/10.1007/s00248-012-0081-3

875 Wrage, N., Velthof, G. L., Van Beusichem, M. L., & Oenema, O. (2001). Role of nitrifier
876 denitrification in the production of nitrous oxide. Soil Biology and Biochemistry, Vol. 33,
877 pp. 1723–1732. https://doi.org/10.1016/S0038-0717(01)00096-7

878 Yang, C., Hamel, C., & Gan, Y. (2015). Incongruous variation of denitrifying bacterial

879 communities as soil N level rises in Canadian canola fields. Applied Soil Ecology, 89(3),
880 93–101. https://doi.org/10.1016/j.apsoil.2015.01.002

881 Zumft, W.G., 1997. Cell biology and molecular basis of denitrification? Microbiol. Mol. Biol.
882 Rev. 61, 533–616.

Figure1

Click here to download Figure: Fig1.pdf

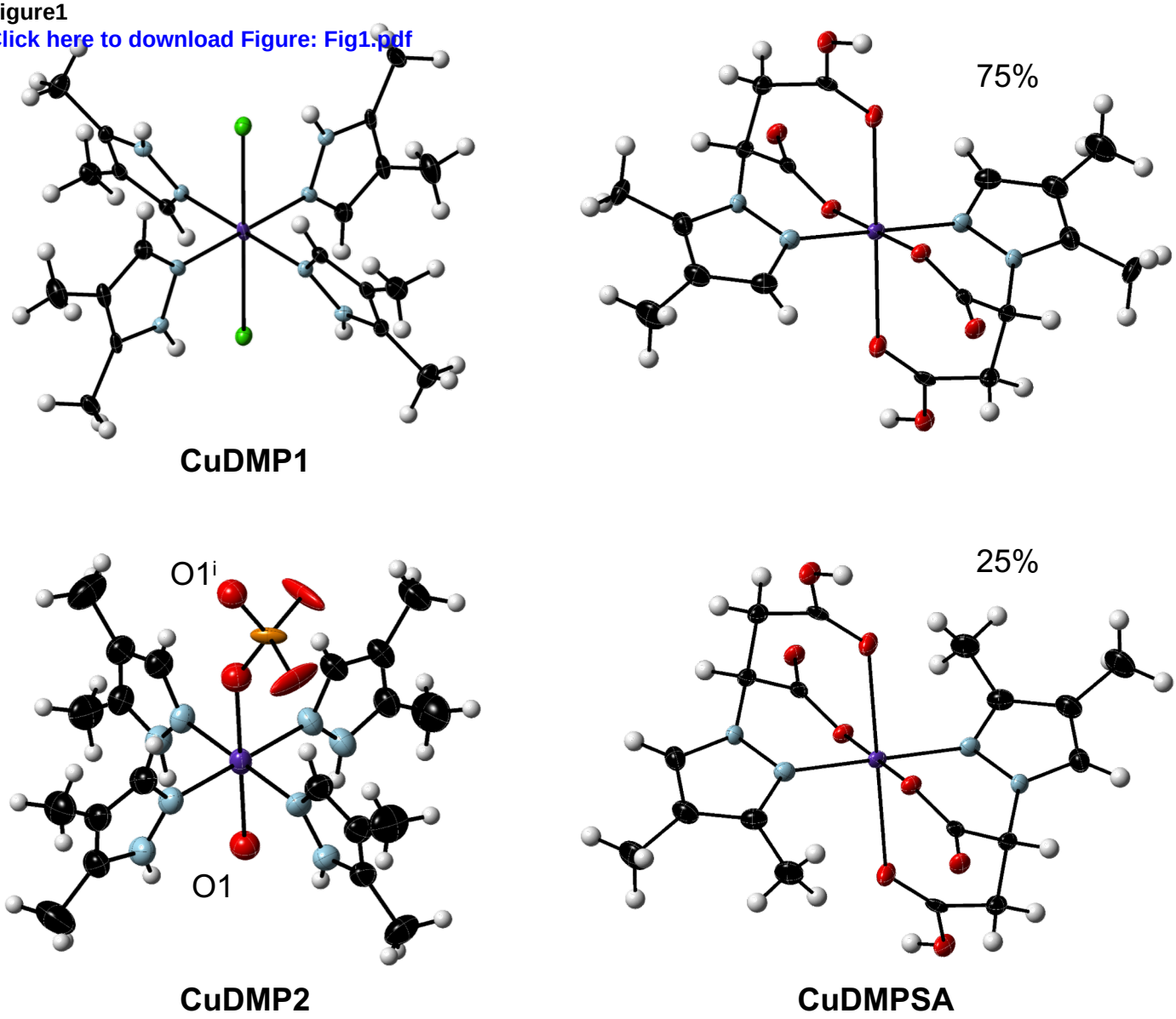

Figure 1. ORTEP views of **CuDMP1**, **CuDMP2** and **CuDMPSA** showing 50% probability displacement ellipsoids. The two isomers of DMPSA that coexist in the structure of **CuDMPSA** are represented independently. Color code: Cu, violet; C, black; Cl, green; H, white; N, blue; O, red; S, orange. Symmetry code: i) x, 1+y, z.

Figure2

Click here to download Figure: Fig2.pdf

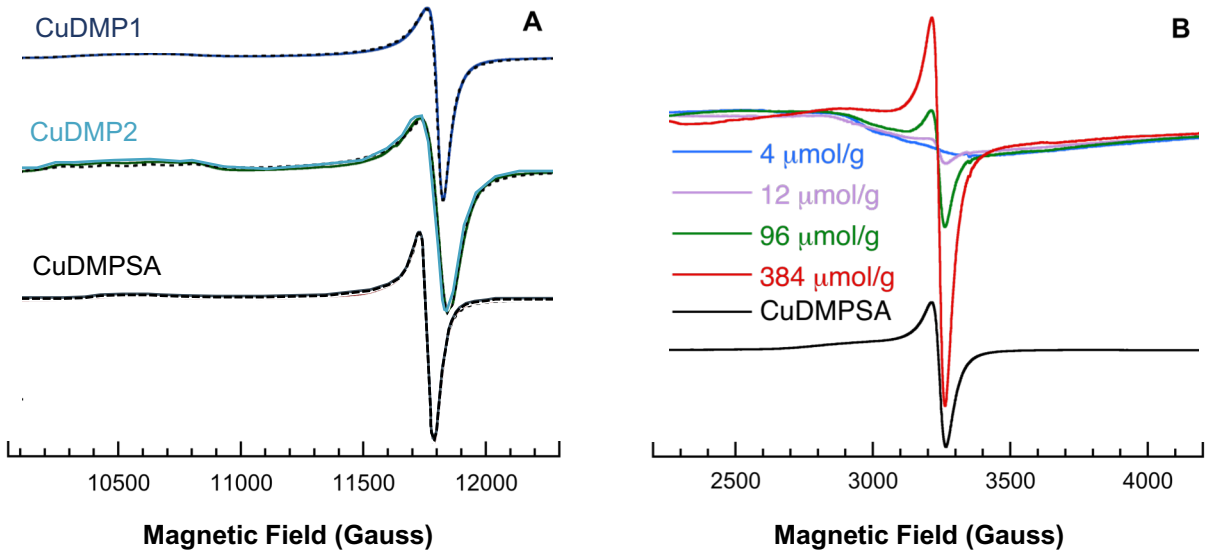

Figure 2. A) Experimental and simulated Q-band (33.9 GHz) EPR spectra of **CuDMP1**, **CuDMP2** and **CuDMPSA**. **B)** Room temperature X-band (9.40 GHz) EPR spectra of soils with different Cu content.

Figure3

Click here to download Figure: Fig3.pdf

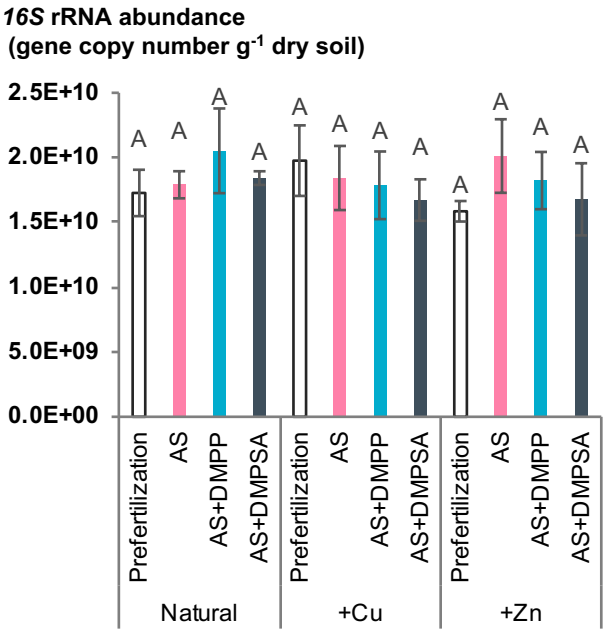

Figure 3. Total bacterial abundance expressed as *16S rRNA* gene copy number per gram of dry soil. Different letters indicate significant differences using the Duncan Test ($P < 0.05$; n = 3).
AS = Ammonium sulphate 21%; DMPP = 3,4-dimethyl-1H-pyrazole phosphate; DMPSA = 2-(3,4-dimethyilpyrazole-1-YL)-succinic acid; Natural = soil with no-added metals; +Cu = natural soil + 8 mg Cu kg^{-1} dry soil; +Zn = natural soil + 8 mg Zn kg^{-1} dry soil.

Figure4

Click here to download Figure: Fig4.pdf

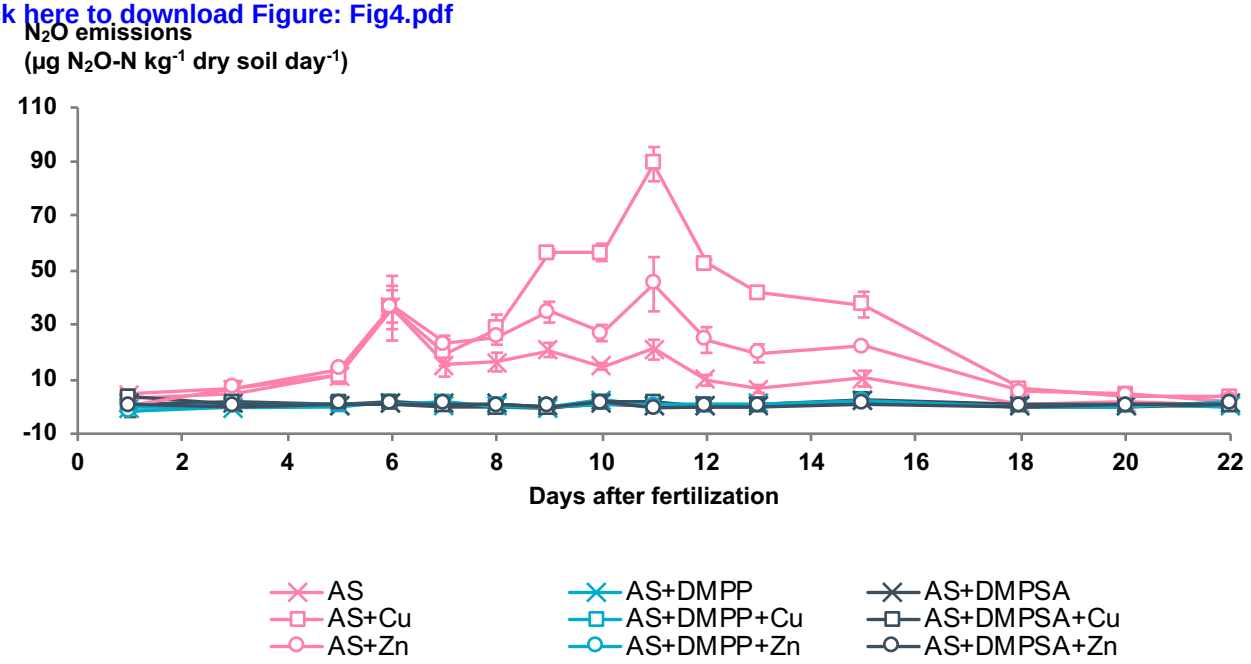

Figure 4. N_2O daily emissions from soil expressed as µg N_2O-N per kg of dry soil and day.
AS = Ammonium sulphate 21%; DMPP = 3,4-dimethyl-1H-pyrazole phosphate; DMPSA = 2-(3,4-dimethyilpyrazole-1-YL)-succinic acid; +Cu = natural soil + 8 mg Cu kg^{-1} dry soil; +Zn = natural soil + 8 mg Zn kg^{-1} dry soil.

Figure5

Click here to download Figure: Fig5.pdf

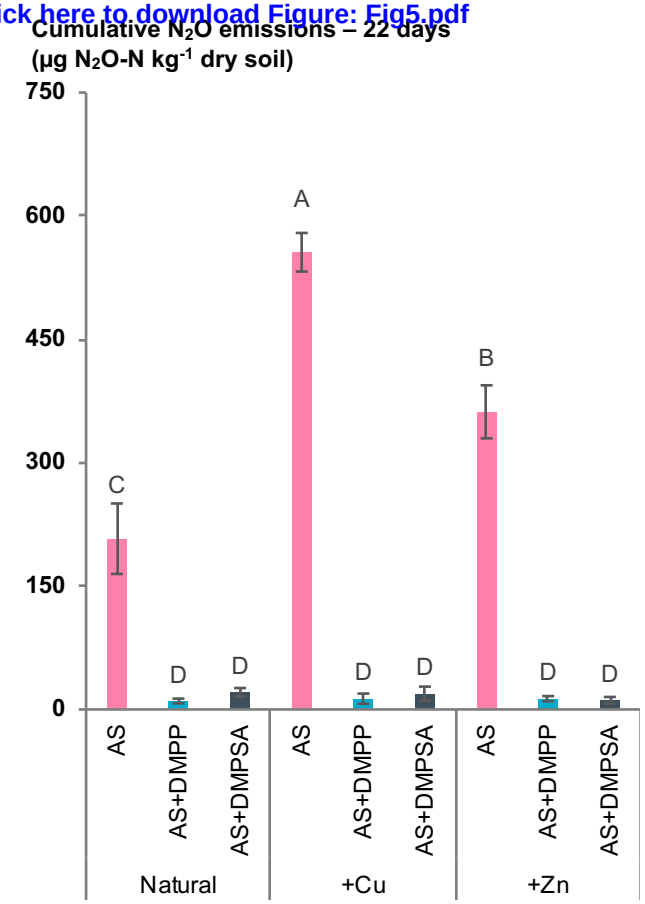

Figure 5. Total cumulative N_2O emissions from soil expressed as µg N_2O-N per kg of dry soil. Different letters indicate significant differences using the Duncan Test ($P < 0.05$; n = 3).

AS = Ammonium sulphate 21%; DMPP = 3,4-dimethyl-1H-pyrazole phosphate; DMPSA = 2-(3,4-dimethyilpyrazole-1-YL)-succinic acid; Natural = soil with no-added metals; +Cu = natural soil + 8 mg Cu kg^{-1} dry soil; +Zn = natural soil + 8 mg Zn kg^{-1} dry soil.

Figure6

Click here to download Figure: Fig6.pdf

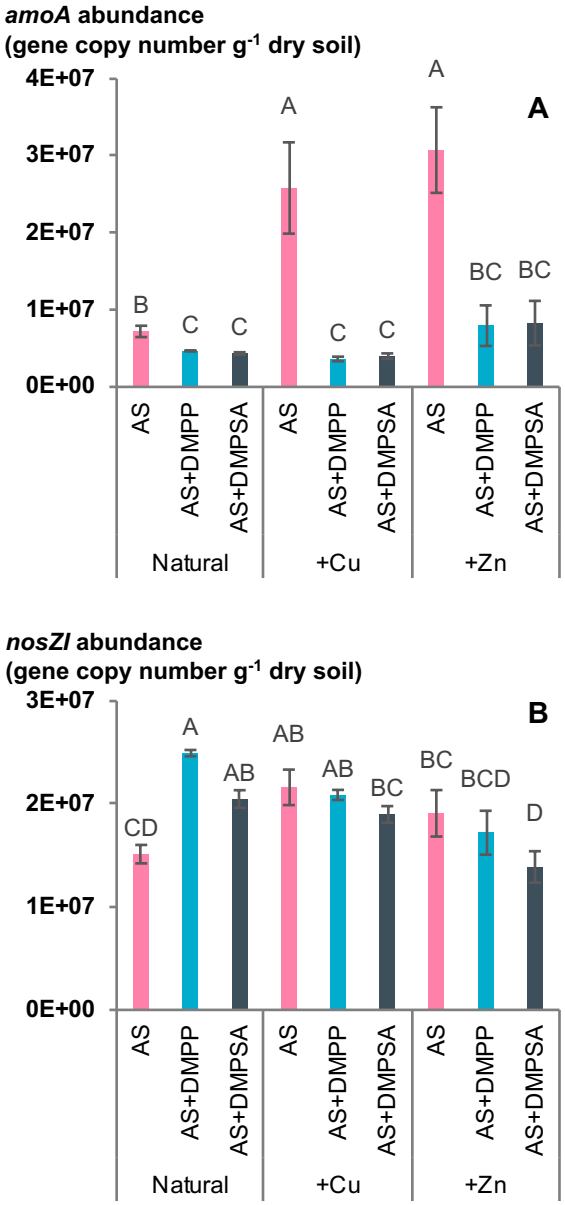

Figure 6. **A)** AOB abundance and **B)** N_2O-RD abundance, expressed respectively as *amoA* and *nosZI* gene copy number per gram of dry soil. Different letters indicate significant differences using the Duncan Test ($P < 0.05$; n = 3). AS = Ammonium sulphate 21%; DMPP = 3,4-dimethyl-1H-pyrazole phosphate; DMPSA = 2-(3,4-dimethyilpyrazole-1-YL)-succinic acid; Natural = soil with no-added metals; +Cu = natural soil + 8 mg Cu kg^{-1} dry soil; +Zn = natural soil + 8 mg Zn kg^{-1} dry soil.

Supplementary tables and figures

Click here to download Supplementary material for on-line publication only: Supplementary-material.pdf

Credit Author Statement

Mario Corrochano-Monsalve: Conceptualization, Investigation, Formal analysis, Visualization, Writing – Original Draft, Supervision. **Carmen González-Murua**: Conceptualization, Supervision, Project administration, Funding acquisition. **Adrián Bozal-Leorri**: Conceptualization, Investigation. **Luis Lezama**: Conceptualization, Formal analysis, Resources. **Beñat Artetxe**: Conceptualization, Resources, Formal analysis, Visualization, Writing – Original Draft, Supervision. All the authors contributed to the discussion of the results and the final edition of the manuscript.

***Declaration of Interest Statement**

Declaration of interests

☒ The authors declare that they have no known competing financial interests or personal relationships that could have appeared to influence the work reported in this paper.

☐The authors declare the following financial interests/personal relationships which may be considered as potential competing interests: